Appl. Phys. B 68, 377–381 (1999)

Applied Physics B
Lasers
and Optics

Invited paper

Decay and dephasing of image-potential states due to surface defects and disorder

M. Weinelt[1], Ch. Reuß[1], M. Kutschera[1], U. Thomann[1], I.L. Shumay[1], Th. Fauster[1], U. Höfer[2,3], F. Theilmann[4], A. Goldmann[4]

[1] Lehrstuhl für Festkörperphysik, Universität Erlangen, D-91058 Erlangen, Germany
[2] Max-Planck-Institut für Quantenoptik, D-85740 Garching, Germany
[3] Physik Department, Technische Universität München, D-85747 Garching, Germany
[4] Fachbereich Physik, Universität Kassel, D-34131 Kassel, Germany
(Fax: +49-9131/852-8400, E-mail: Weinelt@fkp.physik.uni-erlangen.de)

Received: 19 October 1998

Abstract. The dynamics of electrons in image-potential states has been studied by means of time- and energy-resolved two-photon photoemission. The loss of coherence in quantum-beat spectroscopy shows directly the influence of pure dephasing which can be determined also from the difference between the results of linewidth and decay rate measurements. We present several examples for the correlation of decay and dephasing with surface defects and disorder.

PACS: 73.20.At; 79.60.Dp; 79.60.Ht

The properties of electrons at surfaces and interfaces of solids are of both fundamental and technological interest [1–4]. The availability of ultrashort laser pulses has opened the way to direct time-domain investigations of electron dynamics. A particularly powerful experimental technique for surface studies is time-resolved two-photon photoemission (2PPE) [1, 5]. Electrons are excited with a pump pulse into an intermediate state below the vacuum level and are subsequently photoemitted by a second time-delayed probe pulse (see Fig. 1). Angle-resolved photoemission yields energy and momentum resolution, while the pump-and-probe technique allows one to study the time-dependent relaxation behavior.

Recently, it has been demonstrated that by exploiting coherence phenomena phase information about the involved wave functions can also be extracted with 2PPE. This becomes possible either by controlling the time delay between pump and probe pulses with interferometric precision [5] or by coherently exciting a superposition of eigenstates, i.e. an electronic wave packet [6]. For these schemes to work, it is not only necessary that the excited states have a suffiently long lifetime but also that their coherence is not rapidly destroyed by quasi-elastic scattering events (so-called pure dephasing). The most important scattering events, which – under conditions of low excitation densities – lead to pure dephasing, are due to the interaction with phonons and with defects or impurities. While some information about electron–phonon interaction as well as about defect and impurity scattering of occupied surface states has been deduced from careful analysis of photoemission lineshapes [2], very little is known about phase-breaking scattering events of excited or coherent electronic states.

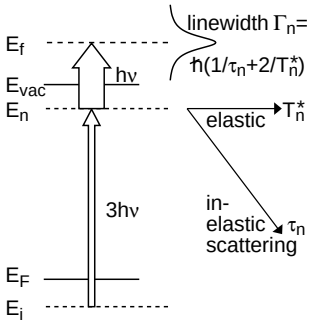

Fig. 1. Schematic representation of bichromatic 2PPE. The population of the intermediate state decays with the lifetime τ_n. The linewidth contains additional contributions from dephasing $2\hbar/T_n^*$

In general, the coherent excitation of energetically close but separated levels leads to quantum interference between these states. As a consequence, a quantum-beat pattern is observed directly in the delay-dependent intensity variation of the photoemission signal [6]. In the absence of events that lead to pure dephasing, the temporal evolution of the wave packet is governed by the initial phase relationship and the decay rate of the states involved.

In the presence of quasi-eleastic scattering events which leave the electron in its excited state but destroy its phase coherence, the observed quantum interference is damped faster than the overall intensity decays. Quantum-beat spectroscopy thus provides a very direct means to study both quasieleastic and inelastic scattering processes of electrons at surfaces by 2PPE [7]. An alternative approach is based on the comparison of energy- and time-domain 2PPE experiments. In the case of uncorrelated scattering events both elastic and inelastic processes lead to a Lorentzian lineshape with a full width at half maximum of $\Gamma_n = \hbar(1/\tau_n + 2/T_n^*)$. For sufficiently short pump and probe pulses the decay rate of the signal in time-resolved 2PPE directly yields the lifetime τ_n, and the pure dephasing time T_n^* can be deduced [7, 8].

In this article we summarize our recent investigations of the image-potential states of CO/Cu(100) and Cu/Cu(100) where several aspects of decay and dephasing induced by ordered and disordered adsorbate layers have been addressed. The results demonstrate that single-crystal surfaces offer a relatively simple way to manipulate electronic dephasing and decay rates by the controlled adsorption of adatoms and molecules.

Image-potential states are a class of normally unoccupied electronic states that can be observed at a variety of single-crystal metal surfaces [9, 10]. These states are trapped in the potential well formed by the Coulomb-like attractive image potential and the repulsive barrier of the metal due to the band gap in the projected bulk band structure. The resulting eigenstates form a Rydberg series converging towards the vacuum level E_{vac} (see Fig. 1) with energies

$$E_n = E_{\mathrm{vac}} - 0.85\,\mathrm{eV}/(n+a)^2,\ n = 1, 2, \ldots .$$

The quantum defect a accounts for the influence of the band structure at the surface. For the clean surface the electron motion parallel to the surface is usually little influenced by the surface potential and the electron behaves like a particle with the free-electron mass m. Because the wave function is mainly located in the vacuum and its penetration into the metal is attenuated by the band gap, typical lifetimes of image-potential states can range from some 10 fs ($n = 1$) up to several ps (higher n). These long lifetimes together with the close energetic spacing for states with higher quantum numbers are prerequisites for the observation of the coherent phenomena described above.

1 Experiment

The frequency-tripled radiation of a Ti:sapphire laser was used as a pump pulse, whilst the fundamental radiation was used as probe pulse. Typical pulse widths were 75 fs and 45 fs, respectively. The electrons were detected normal to the surface by means of a hemispherical energy analyzer. Energy and angular resolution are 40 meV and $\pm 0.6^\circ$, respectively. For details of the experimental setup see [11, 12]. All spectra were recorded at 90 K in order to keep contributions from electron–phonon scattering small [8, 13, 14]. Thereby, changes in the phonon spectra, e.g. due to CO adsorption, can also be neglected. The Cu samples were prepared by standard techniques. CO adsorption was monitored via LEED using a full-screen video system [7]. The evaporation rate and coverage of Cu were calibrated via a quartz microbalance.

2 The role of defects

As mentioned above, the individual contributions of decay and dephasing can be directly visualized by time-resolved coherent 2PPE spectroscopy of higher-order image-potential states.

Spectra for the Cu(100) sample without and with small CO coverages are depicted in Fig. 2. For these measurements the electron energy analyzer was tuned close to the energy of the $n = 3$ image-potential state and the 2PPE intensity was recorded as a function of pump-probe delay, respectively. The

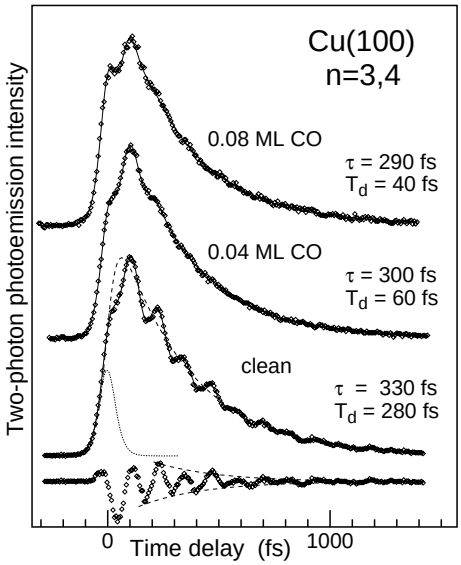

Fig. 2. The coherent excitation of the $n = 3$ and $n = 4$ image-potential states leads to quantum beats superimposed on the decay of the $n = 3$ population (*dashed line in lower spectrum*). The *difference curve* at the bottom illustrates the decay of the phase coherence. The *dotted line* shows the cross-correlation between pump and probe pulse

coherent superposition of the $n = 3$ and $n = 4$ image-potential states leads to oscillations with a period of 117 fs superimposed on the exponential decay of the population (lifetime $\tau_3 \approx \tau \simeq 330$ fs). For the clean Cu surface the decay of these quantum beats (Fig. 2, bottom) occurs with a time constant T_{d} of $\simeq 280$ fs. As the number of defects, i.e. the number of CO molecules randomly distributed on the surface, increases, the dephasing rate $2\hbar/T_{\mathrm{d}}$ also increases. As seen from the upper curves in Fig. 2, even a small amount of CO molecules (4% of a monolayer (ML)) is sufficient to effectively destroy the initial phase coherence. Oscillations are now only visible up to 200 fs delay corresponding to a dephasing time T_{d} of 60 fs. While the dephasing rate increases drastically for small coverages, the lifetime τ changes only slightly.

The decay rate $\hbar/\tau_n$ of the $n = 1$, 2, and 3 image-potential states derived from similar time-resolved measurements is depicted in Fig. 3. The transient 2PPE response of the occupied

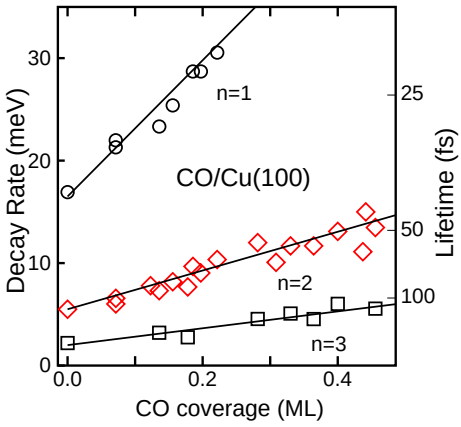

Fig. 3. Decay rate of the $n = 1, 2$, and 3 image-potential states for CO/Cu(100) vs. CO coverage

surface state on Cu(111) was routinely used to evaluate the cross-correlation of pump and probe pulse (see dotted line in Fig. 2), which is essential for the accurate determination of short lifetimes. Up to ≈ 0.4 ML CO coverage the decay rate increases linearly with CO coverage, suggesting that the unoccupied CO related states in the band gap provide additional decay channels [15, 16].

Evidently, the slope depends on the quantum number n. The change of the decay rate with coverage is summarized in Fig. 4. The observed n dependence parallels that for the decay rate of the clean surface. We therefore anticipate similar decay mechanisms [7, 9].

For the well-separated low-n image-potential states the pulse duration of the excitation pulse of 75 fs is too long to simultaneously excite several states. In this case the elastic scattering contributions to the linewidth were extracted from the comparison of time- and energy-resolved spectra. For low coverages linewidth and decay rate increase linearly with CO exposure. From the difference of the average slopes we deduce a change of dephasing rate of 450 ± 150 meV/ML for the $n = 1$ state [7] (see also Fig. 7).

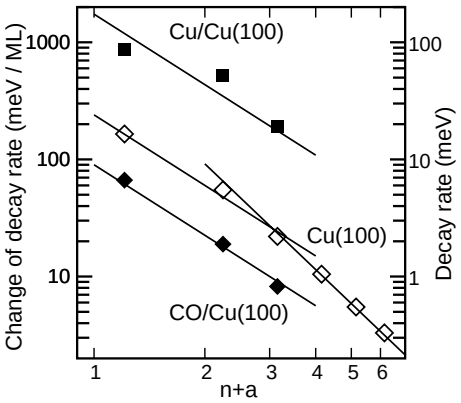

Fig. 4. Change of decay rate for CO/Cu(100) and Cu/Cu(100) vs. quantum number $n + a$ for the lowest image-potential states. The *open symbols* show the decay rate for the clean surface

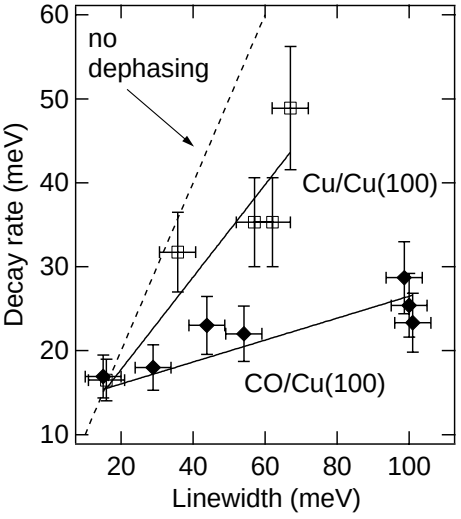

Fig. 5. Decay rate vs. linewidth for CO/Cu(100) and Cu/Cu(100). The *dashed line* indicates the expected linewidth without dephasing

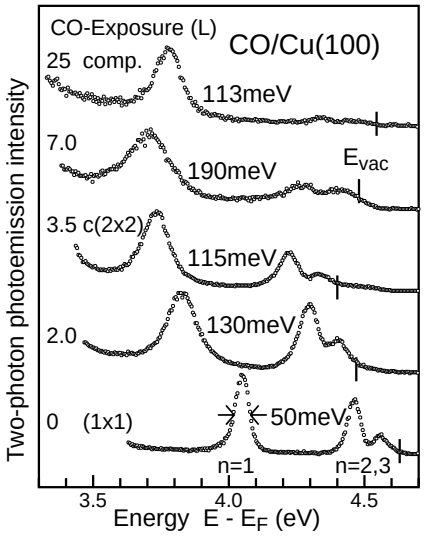

Fig. 6. Series of energy-resolved 2PPE spectra as a function of CO exposure

The following simple model allows us to estimate the contribution of a single CO molecule. Because of the large spectral width of the excitation pulse ($\simeq 38$ meV), a certain distribution of states with different momentum $\hbar k_\parallel$ on the image-potential state parabola is coherently excited. The intermediate state probed in normal emission can thus be described as a wave packet with the width $\Delta k_\parallel \simeq 0.1\,\text{Å}^{-1}$ centered at $k_\parallel = 0$. If we assume for simplicity a Gaussian $k_\parallel$-distribution the resulting spatial extension

$$\langle \Delta x \rangle^2 = 1/4\Delta k_\parallel^2 + (\hbar \Delta k_\parallel / m)^2 t^2$$

equals 25 Å^2 for $t = 0$ and spreads to 2200 Å^2 for $t = 40$ fs. Such a dephasing time of 40 fs is observed for the $n = 1$ state at a CO coverage of 0.04 ML and corresponds to about

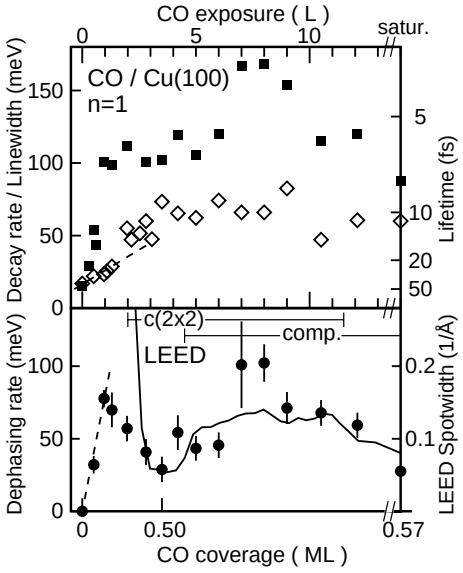

Fig. 7. *Top*: Linewidth (*filled squares*) and decay rate (*open diamonds*) for the $n = 1$ image-potential state on Cu(100) as a function of CO exposure. *Bottom*: Comparison of dephasing rate (*filled circles*, left scale) and LEED spotwidth (*solid line*, right scale). The coverages for the ordered structures are given at the bottom in monolayer units of the clean Cu(100) surface

13 molecules. This very simple model already demonstrates that a few CO molecules are sufficient to destroy phase coherence effectively.

The influence of defects can be further illustrated by Cu homoepitaxy. Copper grows on Cu(100) even at low temperatures in a quasi layer-by-layer mode [17]. This is attributed to the neglegible mobility of Cu atoms at low temperatures [18] and implies single adatoms and/or small island sizes at low coverages. Similar to the case of CO adsorption, a linear increase of the decay rate for increasing coverage below 0.05 ML is observed and is again attributed to additional decay channels. While the n dependence is similar to those observed for clean and CO-covered surfaces, the absolute values of the slope are more than one order of magnitude larger (see Fig. 4). This implies that the coupling to Cu-induced defect states is extremely efficient. For further illustration we compare in Fig. 5 lifetimes and linewidths for data taken at low coverages. In contrast to CO/Cu(100), the decay rate for Cu/Cu(100) contributes significantly to the linewidth. Comparison to the dashed line in Fig. 5 (representing no dephasing) reveals a fraction of about 13% for CO and 55% for Cu. From the combination of the data in Fig. 4 and Fig. 5 we estimate an upper limit for the dephasing rate of 740 meV/ML for Cu-induced defects. Thus, while the dephasing rate for CO and Cu are comparable, the decay rates differ by more than one order of magnitude. As already discussed, small numbers of CO molecules or Cu adatoms are both believed to be randomly distributed on the surface. This allows one to exclude surface morphology as the main cause of the observed different decay rates.

It is therefore evident that dephasing and decay rate are governed by different scattering mechanisms. In other words, elastic and inelastic scattering probe different surface properties.

3 The influence of surface order

Besides modeling different properties of surface defects, the adsorbate systems studied allow one to correlate surface order to dephasing and decay.

Figure 6 shows a series of energy-resolved spectra of the $n = 1, 2$, and 3 image-potential states. In contrast to the linear increase at low coverages, the linewidth of the $n = 1$ image-potential state varies non-monotonically for higher CO exposures. Minima of the linewidth are found at 0, 3.5 L (1 L $= 10^{-6}$ Torr s), and saturation-exposure. For these exposures the well-ordered surface structures (1×1), c(2×2) and a compressed $(7\sqrt{2} \times \sqrt{2})$R45° structure are formed [19]. By a combination of linewidth and decay rate (see top part of Fig. 7) the dephasing rate is extracted. A detailed LEED analysis [7] allows one to quantitatively correlate surface order and dephasing. The spotwidth of the LEED superstructure spots and the dephasing rate depicted in the lower part of Fig. 7 exhibit virtually the same coverage dependence. This supports the picture where pure dephasing is caused by quasielastic scattering of the electron in the intermediate state. For less-ordered overlayers the increase in spotwidth is caused by scattering events with small momentum transfer.

The same momentum-change will give rise to dephasing of an electron in the image-potential state. The inverse of the dephasing rate and LEED spotwidth represent the time and distance between two quasielastic scattering events of the electron in the intermediate state. The proportionality introduces an average speed $v \simeq 50\,\text{meV}/(\hbar\, 0.1\,\text{Å}^{-1}) = 0.76\,\text{Å/fs}$. This speed agrees nicely with the velocity $v = \hbar\Delta k/m = 1.15\,\text{Å/fs}$ that describes the spread of the Gaussian wave packet described above.

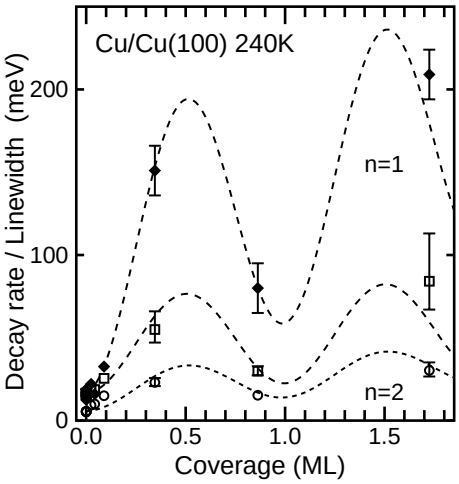

Fig. 8. Linewidth (*filled diamonds*) and decay rate (*open squares*) for the $n = 1$ and decay rate for the $n = 2$ (*open circles*) image-potential state as a function of Cu-coverage. The films were annealed to 240 K, deposition and measurements were performed at 100 K

A somewhat different situation is found for Cu homoepitaxy. As quasi layer-by-layer growth is observed even at low temperatures, the surface order oscillating with Cu coverage. As expected, upon completion of one monolayer the linewidth of the $n = 1$ image-potential state decreases (Fig. 8). This is again partially due to the decrease of the dephasing rate with increasing surface order.

In addition, we observe a comparable decrease of the decay rate of the $n = 1$ and $n = 2$ image-potential states. This is not surprising, since for quasi layer-by-layer growth the clean-surface situation is nearly regained with the completion of one monolayer and the number of disorder-induced defect states will decrease accordingly.

4 Conclusions

We have investigated how defects and surface order affect lifetime and dephasing rate of image-potential states. The increase in decay rate can be directly related to the number of induced unoccupied adsorbate states, i.e. the number of inelastic scattering channels. While the absolute values vary strongly with the system studied, the dependence on the image-potential state quantum number n shows quite a similar behavior. This suggests that excited-state lifetimes are strongly related to the details of the adsorbate–substrate electronic band structure. Correlating dephasing and surface order reveals that the main contribution to the dephasing rate is quasielastic scattering. This is further demonstrated for higher order image-potential states, where dephasing was directly probed by coherent time-resolved 2PPE.

Acknowledgements. Support by the Deutsche Forschungsgemeinschaft is gratefully acknowledged.

References

1. R. Haight: Surf. Sci. Rep. **21**, 275 (1995)
2. R. Matzdorf: Surf. Sci. Rep. **30**, 153 (1997)
3. R.M. Osgood, Jr., X.Y. Wang: In *Solid State Physics*, Vol. 51, ed. by H. Ehrenreich, F. Spaepen (Academic, San Diego 1997) p. 1
4. C.B. Harris, N.-H. Ge, R.L. Lingle, Jr., J.D. McNeill, C.M. Wong: Annu. Rev. Phys. Chem. **48**, 711 (1997)
5. H. Petek, S. Ogawa: Prog. Surf. Sci. **56**, 239 (1997)
6. U. Höfer, I.L. Shumay, Ch. Reuß, U. Thomann, W. Wallauer, Th. Fauster: Science **277**, 1480 (1997)
7. Ch. Reuß, I.L. Shumay, U. Thomann, M. Kutschera, M. Weinelt, Th. Fauster, U. Höfer: Phys. Rev. Lett. **82**, 153 (1999)
8. E. Knoesel, A. Hotzel, M. Wolf: J. Electron Spectrosc. Relat. Phenom. **88**–**91**, 577 (1998)
9. P.M. Echenique, J.B. Pendry: Prog. Surf. Sci. **32**, 111 (1990)
10. Th. Fauster, W. Steinmann: In *Photonic Probes of Surfaces*, Vol. 2 of *Electromagnetic Waves: Recent Developments in Research*, Chap. 8, ed. by P. Halevi (North-Holland, Amsterdam 1995) p. 347
11. I.L. Shumay, U. Höfer, Ch. Reuß, U. Thomann, W. Wallauer, Th. Fauster: Phys. Rev. B **58**, 13974 (1998)
12. U. Thomann, I.L. Shumay, M. Weinelt, Th. Fauster: Appl. Phys. B **68**, 531 (1999)
13. B.A. McDougall, T. Balasubramanian, E. Jensen: Phys. Rev. B **51**, 13891 (1995)
14. R. Matzdorf, G. Meister, A. Goldmann: Phys. Rev. B **54**, 14807 (1996)
15. J. Rogozik, V. Dose, K.C. Prince, A.M. Bradshaw, P.S. Bagus, K. Hermann, P. Avouris: Phys. Rev. B **32**, 4296 (1985)
16. K.-D. Tsuei, P.D. Johnson: Phys. Rev. B **45**, 13827 (1992)
17. W.F. Egelhoff, Jr., I. Jacob: Phys. Rev. Lett. **62**, 921 (1989)
18. J.J. deMiguel, A. Sanchez, A. Cebollada, J.M. Gallego, J. Ferron, S. Ferrer: Surf. Sci. **189**/**190**, 1062 (1987)
19. P. Uvdal, P.-A. Karlsson, C. Nyberg, S. Andersson, N.V. Richardson: Surf. Sci. **202**, 167 (1988)